GA–A26899

EXPERIMENT AND MODELING OF ITER DEMONSTRATION DISCHARGES IN THE DIII-D TOKAMAK

by

J.M. PARK, E.J. DOYLE, J.R. FERRON, C.T. HOLCOMB,
G.L. JACKSON, L.L. LAO, T.C. LUCE, L.W. OWEN, M. MURAKAMI,
T.H. OSBORNE, P.A. POLITZER, R. PRATER and P.B. SNYDER

OCTOBER 2010

GENERAL ATOMICS

DISCLAIMER

GA–A26899

EXPERIMENT AND MODELING OF ITER DEMONSTRATION DISCHARGES IN THE DIII-D TOKAMAK

by
J.M. PARK[1], E.J. DOYLE[2], J.R. FERRON, C.T. HOLCOMB[3], G.L. JACKSON, L.L. LAO, T.C. LUCE, L.W. OWEN[1], M. MURAKAMI[1], T.H. OSBORNE, P.A. POLITZER, R. PRATER and P.B. SNYDER

This is a preprint of a paper to be presented at the 23rd IAEA Fusion Energy Conference, October 11–16, 2010 in Daejon, Republic of Korea and to be published in Proceedings.

[1]Oak Ridge National Laboratory, Oak Ridge, Tennessee
[2]University of California, Los Angeles, California
[3]Lawrence Livermore National Laboratory, Livermore, California

Work supported in part by
the U.S. Department of Energy
under DE-AC05-00OR22725, DE-FG02-08ER54984,
DE-FC02-04ER54698, DE-FG02-95ER54309
and DE-AC52-07NA27344

GENERAL ATOMICS ATOMICS PROJECT 30200
OCTOBER 2010

ABSTRACT

DIII-D is providing experimental evaluation of four leading ITER operational scenarios: the baseline scenario in ELMing H-mode, the advanced inductive scenario, the hybrid scenario, and the steady state scenario. The anticipated ITER shape, aspect ratio, and value of I/aB have been reproduced, with the size reduced by a factor of 3.7, while matching key performance targets for β_N and H_{98}. Since 2008, substantial experimental progress has been made in improving the match to other expected ITER parameters for the baseline scenario. A lower density baseline discharge has been developed with improved stationarity and density control to match the expected ITER edge pedestal collisionality (ν_e^*~0.1). Target values for β_N and H_{98} were maintained at lower collisionality (lower density) operation without loss in fusion performance but with significant change in ELM characteristics. The effects of lower plasma rotation were investigated by adding counter-neutral beam power, resulting in only a modest reduction in confinement. Robust preemptive stabilization of 2/1 NTMs was demonstrated for the first time using ECCD under such ITER-like conditions. Data from these experiments have been used extensively to test and develop theory and modeling for realistic ITER projection and for further development of its optimum scenarios in DIII-D. Theory-based modeling using TGLF with an experimental edge pedestal boundary condition reproduces T_e and T_i profiles reasonably well for the ITER scenarios developed in DIII-D. Modeling of the baseline scenario for low and high density discharges indicates that the transport mechanism will change dramatically in the ITER relevant regime of low collisionality and electron dominant heating. A modest performance increase of ~15% is needed to compensate for the expected lower rotation of ITER. Modeling of the steady-state scenario reproduces the strong dependence of confinement, stability, and noninductive fraction (f_{NI}) on q_{95}, as found in the experimental I_p scan, indicating that optimization of the q-profile is critical to simultaneously achieving the f_{NI}=1 and Q=5 goals.

1. INTRODUCTION

The DIII-D program is providing suitably scaled experimental evaluations of the four primary ITER operational scenarios [1]. The four ITER scenarios, which have been demonstrated, are: the baseline scenario in ELMing H-mode, the advanced inductive scenario, the hybrid scenario, and the steady state scenario [2]. Unique features of this work are that the plasmas incorporate as constraints leading operational features of the ITER scenarios, such as the design values for the ITER plasma cross-section, aspect ratio, and I/aB. Key aspects of all four of these scenarios have been replicated successfully on DIII-D, providing an improved and unified physics basis for transport [3] and stability [4,5] modeling, as well as performance extrapolation to ITER [6]. In all four scenarios performance equals or closely approaches that required to realize the physics and technology goals of ITER. This paper will present recent progress on the ITER demonstration experiments made since 2008 IAEA and integrated theory-based modeling for projection to ITER and optimum ITER scenario development in DIII-D based on the key findings from the ITER demonstration experiment.

2. ITER BASELINE SCENARIO

Conventional ELMy H-mode plasmas have been operated at a normalized plasma current $I_N \equiv I(MA)/a(m)B(T)$ value of 1.415, corresponding to 15 MA operation on ITER. The resulting value of q_{95} = 3.1, close to the ITER design value of 3.0. The plasma was operated with feedback control of the NBI power to maintain the ITER target of β_N=1.8. Confinement was at or above the ITER target of H_{98}=1.0. Recent attention has focused on improving the match to the anticipated characteristics for the ITER baseline scenario such as edge pedestal collisionality and plasma rotation. A lower density baseline discharge was developed to match the expected ITER edge pedestal collisionality (ν_e^*~0.1). The density was reduced by a factor 2 and the temperatures raised by lowering I_p and applying electron cyclotron heating (ECH), while keeping the same I/aB =1.415 and T_e/T_i~1. Here, ECH is multi purpose, suppressing 2/1 neoclassical tearing mode (NTM) using EC current drive, thereby avoiding rotational locking with its loss of confinement and possible disruption. Additional ECH with reduced NB power changes the confinement characteristics due to dominant electron heating. A higher density discharge reaches the ITER absolute density of $1 \times 10^{20} m^{-3}$ or n/n_{GW} ~ 0.65 (ITER target 0.85). Density control and stationarity were improved substantially both in low and high density discharges for the ~$3\tau_R$ duration of the H-mode flattop, which is the same normalized duration as for ITER.

Target values for β_N and H_{98} were maintained at lower density (lower collisionality) without loss in fusion performance. The time evolution of the main plasma parameters for such a lower density discharge is illustrated in Fig. 1, compared with a high density discharge. Both high and low collisionality discharges achieve the same global energy confinement measured by ITER confinement scaling (H_{98}~1). The projections to ITER using the model described in Ref. [7] shows that both discharges meet or exceed the ITER target of 400 MW of fusion power and $Q \geq 10$ for Scenario 2. Despite the same global confinement, however, significant change in local transport characteristics was observed, indicating that the transport mechanism will change dramatically in the ITER relevant-regime of low collisionality and electron dominant heating. Figure 2 shows the local thermal diffusivities ($\chi \equiv -q/n\nabla T$) from power balance analysis using ONETWO [8], where the energy loss due to ELMs was separated by taking into account a time derivative term in the energy balance equation using the experimental profiles collected in the same phases between successive ELMs [9]. Linear stability analysis using the trapped gyro-Landau fluid (TGLF) moment equations [10] [Fig. 2(d)] indicates that ion temperature gradient (ITG) and trapped electron mode (TEM) (lower k modes, $k_\theta \rho_i$<1.0) are dominant for lower collisionality discharges, while the electron temperature gradient (ETG) mode (higher k modes, $k_\theta \rho_i$>1.0) prevails for high collisionality discharges. Localized electron heating by ECH increases energy transport significantly at ρ=0.75 for the lower density discharge. Transition of the transport mechanism from ETG to ITG/TEM is more evident when electron heating is significantly higher than ion heating.

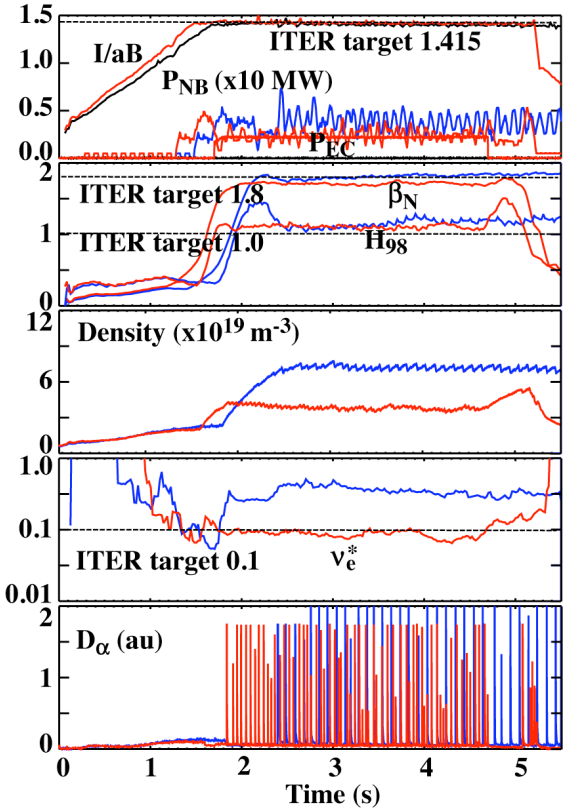

FIG. 1. Key parameters for ITER baseline discharges [high n_e/collisionality (blue), low n_e/collisionality (red)].

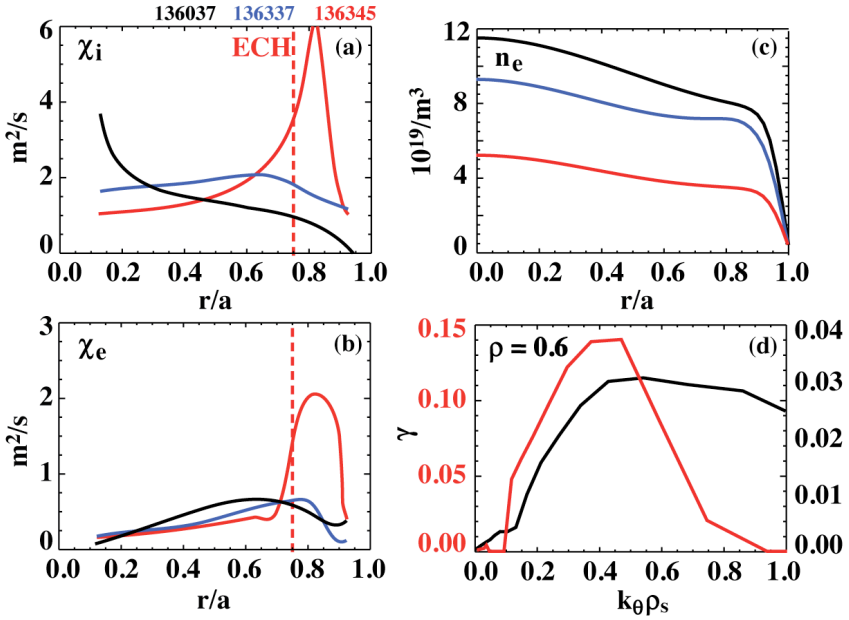

FIG. 2. Power balance thermal diffusivities for (a) ions and (b) electrons for the density (collisionality) scan. (c) density profile, (d) linear growth rate for the most unstable mode at ρ=0.6 from TGLF linear stability analysis. (Red: $\langle n_e \rangle$=3.8x10^{19}m^{-3}, ν_e^*=0.1, blue: $\langle n_e \rangle$=7.2x10^{19}m^{-3}, ν_e^*=0.35, black: $\langle n_e \rangle$=8.9x10^{19}m^{-3}, ν_e^*=0.6.)

TGLF transport simulations [11,12] using FASTRAN [6] reproduce the experiment temperature profiles and the changes in the local transport process as observed in the experiments. The electron (T_e) and ion (T_i) temperature profiles are calculated taking the density and plasma rotation profiles from experimental analysis. The experimental *E*x*B* shearing rate is obtained from the radial electric field profile, which is determined using charge exchange spectroscopy (CER) measurements of the poloidal and toroidal carbon impurity velocities [13]. The boundary condition is taken at ρ=0.84 using the profiles collected from the last 20% of the ELM cycle. The simulation presented here employs TGLF electrostatically in Miller geometry. Figure 3 shows the calculated T_e and T_i profiles compared with the experimental ones. Agreement between calculation and experiment is reasonably good for the range of the density (collisionality) scan. TGLF transport simulation indicates that rotation plays an important role, especially in the lower density discharge. TGLF simulation without the stabilizing effects of *E*x*B* flow shear [14] underestimates the calculated temperature profile significantly as shown in Fig. 4. The calculated TGLF thermal diffusivities show better agreement with the power balance analysis only when the *E*x*B* stabilization is included in the simulation. TGLF simulation show relatively small effects of rotation for higher density discharge, where ETG is dominant in the turbulent transport. The effects of lower plasma rotation were investigated experimentally by adding counter-neutral beam power in low collisionality discharges. Initial data indicates that reduced plasma rotation degrades confinement in the baseline scenario but results in only a modest reduction in confinement. Modest one-fourth counter-beam substantially changes rotation in the region of $\rho > 0.25$ (from 80 krad/s to 30 krad/s at ρ~0.5), resulting in the *E*x*B* shearing rate $\gamma_E \sim 0$ over $0.3 < \rho < 0.6$. The confinement factor H_{98} was reduced by ~15% but the confinement remained close to the target value of H_{98}~1. Both experiment and modeling indicate need for performance margin to account for effects of lower rotation in projecting to ITER.

The density profile is substantially peaked for the baseline discharges, as opposed to the flat density profile assumed in standard ITER profile models [15]. The density peakness for lower density discharge, $<n_e>/n_{e0}$~1.4, is only slightly higher than that of higher density discharge (~1.3) as shown in Fig. 2(c). The density peakness is less sensitive to the collisionality than recent AUG and JET observation [16]. This is partly due to the effects of core particle fueling from NBI. Core fueling for the lower density discharge is a factor of 2 lower due to its reduced injected beam power (from P_{NB}=3.9 MW to 2.2 MW) by adding 2.4 MW of ECH power. Localized ECH at ρ = 0.75 is also likely to pump out particles [17]. The change in ELM characteristics also affects the density peaking as described below. An inward particle pinch for the high density discharges is evident in the particle balance analysis, which is consistent with TGLF modeling and recent gyro-kinetic predictions [18].

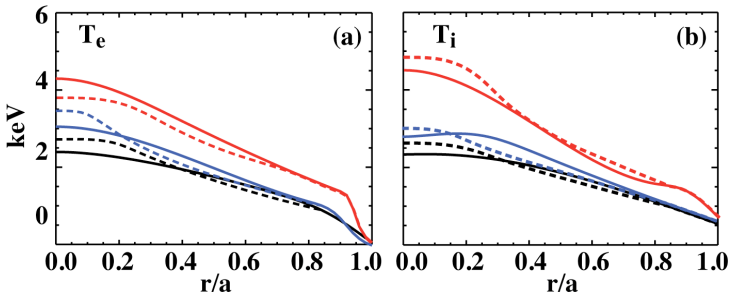

FIG. 3. Comparison of the (a) electron and (b) ion temperature profiles between experiment (solid) and TGLF transport simulation (dashed). Color denotes the same density scan as Fig. 2.

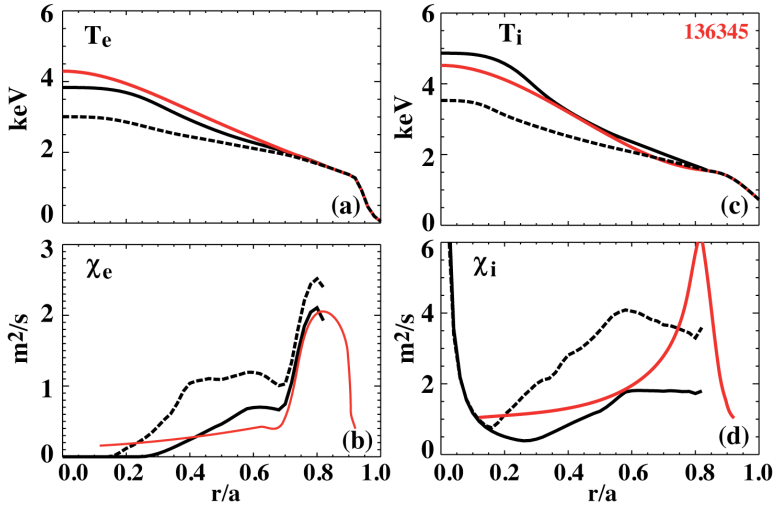

FIG. 4. Comparison of the electron (a,b) and (c,d) ion temperature and thermal diffusivity profiles between experiment (red) and TGLF transport simulation with (black solid) and without (black dashed) *ExB* flow shear stabilization.

One of the important experimental findings is that the lower density discharges that match the anticipated ITER edge pedestal collisionality reveals a significant change in ELM characteristics. The baseline discharge with higher density exhibits large and infrequent (~10 kHz) ELMs [2]. Type I ELMs in such plasmas extent deeply into the core region. The energy loss at ELMs, ΔW_{ELM} is more than 10% of the total stored energy and ~25% of the pedestal energy W_{PED}, which substantially exceeds the ITER limit. As shown in Fig. 1, the lower density discharge shows smaller (~5% of total stored energy) and more frequent (~20 kHz) ELMs. The reduced ELM energy loss appears to be related to the change in the radial extent of ELM affected region [19]. The magnitude of the ELM energy loss and the extent of the ELM affected region are correlated well with the radial region where the peeling-ballooning modes calculated by the ELITE code [20] are unstable. The change in a ratio of the loss power (P_L) to the L-H transition threshold power (P_{TH}) is also likely to play a role in the observed change of the ELM characteristics. It should be noted that high (low) density discharge was operated with P_L/P_{TH}~1 (~3) throughout H-mode phase.

3. STEADY-STATE SCENARIO

One of the primary goals of the ITER project is to demonstrate a reactor scale steady state (SS) operation for the future tokamak reactor [21]. This is very challenging, requiring simultaneous operation with fully noninductive (NI) current drive (noninductive current fraction, f_{NI} = 100%) with fusion gain $Q \geq 5$ and high bootstrap current for pulse length ~3000 s. Steady-state demonstration discharges were operated over a range of $4.5<q_{95}<6.5$ with q_{min}~1.5 using a standard DIII-D prescription [22]. ECCD up to 3MW provides off-axis current drive to keep a hollow current profile. Fully non-inductive operation was obtained at q_{95}=6.5 with β_N~3.1 and f_{BS}~0.7. Loop voltage analysis and transport code simulation show that the inductive current density is small everywhere but with relatively low fusion performance. Duration of fully non-inductive operation is ~$0.7\tau_R$. The fully non-inductive discharges are not stationary, as is evident in time evolution of current profiles, mainly due to limits on the off-axis current drive to maintain the broad current profile. At the highest current with q_{95}~4.5, the discharges were not fully NI, but had fusion performance at the $G \equiv \beta_N H_{89}/q_{95}^2$~0.3 level predicted for Q~5 operation on ITER. Theory-based projection of such discharges to ITER using the scaled edge profile [6] shows a tradeoff between Q and f_{NI} with variation in q_{95}, as observed in DIII-D [Fig. 5(a,b)], indicating that optimization of the q-profile is critical to simultaneously achieving the f_{NI}=1 and Q=5 goals.

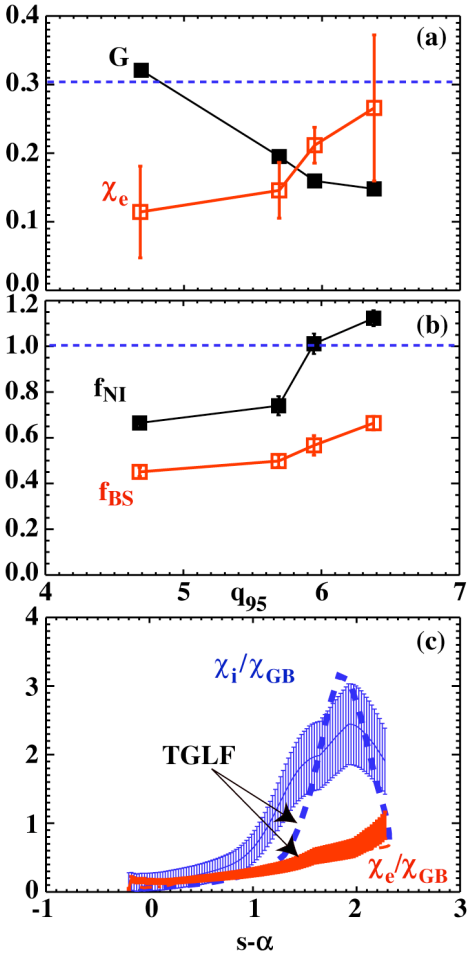

FIG. 5. I_p scan of ITER demonstration discharges for steady-state scenario: (a) Fusion performance (G), electron thermal diffusivity averaged over $0.2<\rho<0.8$ (χ_e), (b) fractions of non- inductive (f_{NI}) and bootstrap (f_{BS}) current as a function of q_{95}. (c) Local thermal diffusivities as a function of magnetic shear, where error bars denote a variation in the discharges for I_p scan.

Experiment and modeling of the steady-state scenario discharges show a strong dependence of confinement, stability, and noninductive fraction (f_{NI}) on q_{95}. The thermal energy confinement time decreases with q_{95}, generally following the scaling of H_{98}, as shown in the averaged electron thermal diffusivity of Fig. 5(a), while f_{NI} and f_{BS} increase with $\beta_N q_{95}$ [Fig. 5(b)]. The edge pedestal provides typically ~40% of the total bootstrap current, and its height and width depend on q_{95}, so that the pedestal plays a key role in optimizing the steady-state scenario. The electron and ion thermal diffusivities appear to correlate mainly with the magnetic shear both in the power balance analysis by TRANSP [23] and in the TGLF modeling [Fig. 5(c)]. TGLF transport simulation using the

same method described in Section 2 reproduces the transport dependency on q_{95} reasonably well for the experimental I_p scan of ITER demonstration discharges, as well as for recent DIII-D experiment for q-profile optimization in double-null shape [24]. Predictive TGLF simulations using model equilibria with a variation of q_{min} and its location, while keeping the pressure profile and q_{95} from experiment, suggest that a larger radius of minimum q with weak magnetic shear can reduce turbulent transport significantly for both electrons and ions. The benefit of weak magnetic shear is evident for a range of $4.5<q_{95}<6.5$ in the TGLF modeling, especially at higher β. Figure 6 compares the calculated n = 1 no- and ideal-wall β_N limit for the experimental I_p scan, which are obtained by using the kinetic profile and equilibrium from experiment as input to the DCON ideal stability code [25]. No noticeable change in the calculated n=1 no-wall limit (β_N~2.8) was observed with variation of q_{95}, while the n=1 ideal wall limit decreases slightly with q_{95}. Predictive modeling using the model equilibrium in the same way as the TGLF modeling indicates strong dependency of the stability limit on q_{min}. At the lowest q_{95}~4.5, the calculated β_N limit decreases with q_{min} for both no- and ideal-wall limits. Conversely, at the highest q_{95}~6.5, the β_N limit increases with q_{min}. The height and width of pedestal decrease with q_{95}, as shown in Fig. 7, which is consistent with EPED prediction [5].

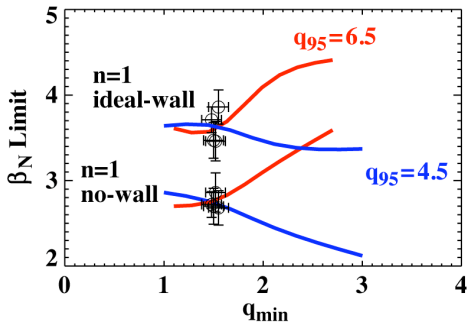

FIG. 6. Dependency of n=1 ideal no- and ideal-wall β_N limit on q_{95} and q_{min}. (Symbol: experimental I_p scan.)

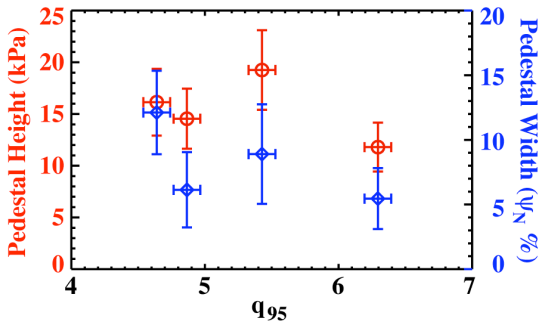

FIG. 7. Dependency of pedestal width (blue) and height (red) on q_{95}.

Integrated theory-based modeling has been carried out to find an optimum q-profile for simultaneously achieving the f_{NI}=1 and Q=5 goals. An iterative numerical procedure is employed that finds a steady state solution (d/dt=0) of core transport (TGLF [12]) using FASTRAN [6] with self-consistent calculation of equilibrium (EFIT [26]) and heating/CD sources (NUBEAM [27], TORAY-GA [28], and CURRAY [29]). The predictive simulation suggests that a larger radius for the minimum of q helps to increase both the fusion performance and f_{NI} at the β_N limit calculated from ideal wall stability, by maximally utilizing the benefits of low magnetic shear and higher pedestal pressure from the increased β_p. A modest improvement of fusion performance was obtained for the q-profile scan ($1.0 < q_{min} < 2.5$) starting from the experimental condition of I_p scan (Fig. 8). At higher q_{95} (lower I_p), even the maximum improvement of plasma confinement factor (~14%) is not sufficient to reach

G=0.3 for the Q=5 goal, indicating that lower q_{95} (higher I_p) operation would be important to reach the f_{NI}=1 and Q=5 goal, simultaneously. A significant increase of f_{BS} is expected at q_{95} = 5.0 with a larger radius of minimum q (q_{min}~2.5) that reaches f_{BS}=0.72 with G=0.3 at the calculated ideal wall stability limit (β_N~3.7). A larger radius of minimum q with weak magnetic shear allows higher β_N operation with improved confinement to increase the bootstrap current fraction, as shown in Fig. 9. The simulations indicate that off-axis current drive is crucial to sustain this favorable q-profile.

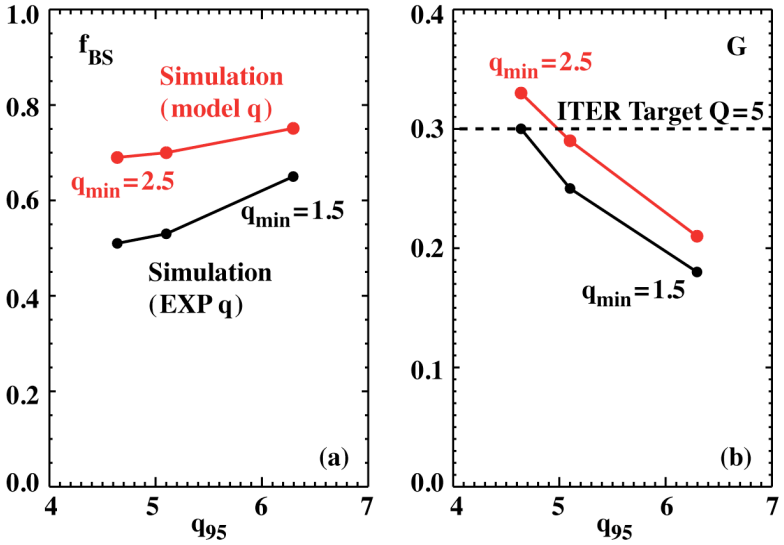

FIG. 8. Integrated theory-based modeling for steady-state ITER demonstration discharge: (a) bootstrap current and (b) fusion performance for q-profile scan.

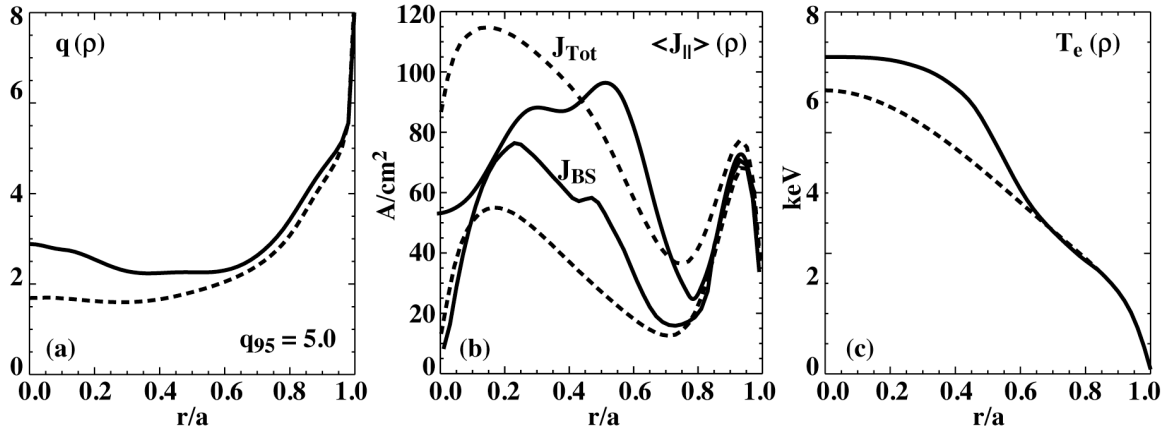

FIG. 9. Comparison of the radial profiles for (a) safety factor, (b) current and (c) electron temperature between q_{min} = 1.5 (dotted) and q_{min} = 2.5 (solid) at q_{95} = 5.0.

4. CONCLUSION

DIII-D is providing experimental evaluation of four leading ITER operational scenarios. Substantial experimental progress has been made in improving the match to the expected ITER parameters for the baseline scenario including edge pedestal collisionality and rotation, which provides invaluable information on many key physics issues such as confinement, transport, and ELM behaviors in ITER relevant regime of low collisionality and rotation. Data from these experiments have been used extensively to test and develop theory and modeling for realistic ITER projection and for further development of its optimum scenarios in DIII-D. Experiment and modeling indicates that ITER will meet or closely approach its two main operational goals: the demonstration of the fusion gain Q>10 for a pulse length of 300-500 s in ELMing H-mode and to achieve simultaneous operation with fully noninductive current drive with the fusion gain Q~5. Strong dependency of confinement, stability and bootstrap fraction on the q-profile indicates that scenario development with optimum current profile is crucial for achieving the fully noninductive Q=5 goal of the steady-state scenario. DIII-D evaluations of ITER scenarios will be further extended by applying new tools such as off-axis NBI [30,31], higher power EC, and fast wave (FW) current drive that will allow extending T_e~T_i operation to more scenarios and developing the steady state scenario with higher fusion performance and bootstrap current fraction.

REFERENCES

[1] Special issue on "Progress in the ITER Physics Basis," Nucl. Fusion **47**, S1 (2007).

[2] DOYLE, E.J., et al., Nucl. Fusion **50**, 75005 (2010).

[3] KINSEY, J.E., et al., "ITER Predictions Using the GYRO Verified and Experimentally Validated TGLF Transport Model," these proceedings, THC/3-3.

[4] GROEBNER, R.J., et al., Nucl. Fusion **49**, 85037 (2009)

[5] SNYDER P.B., et al., Nucl. Fusion **49**, 85035 (2009)

[6] PARK, J.M., et al., 3rd ITPA IOS TG Meeting (Frascati, 2009); MURAKAMI, M., et al., "Integrated Modeling of Steady-state Scenarios and Heating and Current Drive Mixes for ITER," these proceedings, ITR/P1-35.

[7] LUCE, T.C., et al., Phys. Plasmas **11**, 2627 (2004).

[8] ST JOHN, H.E., et al., in Plasma Physics and Controlled Nuclear Fusion Research 1994 (Proc. 15th Int. Conf., Seville, 1994) Vol. 3, p. 603, IAEA, Vienna (1995).

[9] LEONARD, A.W., et al., Nucl. Fusion **47**, 552 (2007).

[10] STAEBLER, G.M., et al., Phys. Plasmas **12**, 102508 (2005).

[11] STAEBLER, G.M., et al., Phys. Plasmas **14**, 055909 (2007).

[12] KINSEY, J.E., et al., Phys. Plasmas **15**, 55908 (2008).

[13] SOLOMON, W.M., et al., Rev. Sci. Instrum. **75**, 3481 (2004).

[14] BURRELL, K.H., et al. Phys. Plasmas 4, 1499 (1997).

[15] POLEVOI, A.R., et al., Nucl. Fusion **45**, 1451 (2005).

[16] ANGIONI, C. et al., Nucl. Fusion, **47,** 1326 (2007).

[17] IDEI, H., et al., Fusion Engineering and Design **26**, 167 (1995)

[18] ANGIONI, C. et al., Phys. Plasmas **14**, 55905 (2007).

[19] SNYDER, P.B. et al., Nucl. Fusion **44**, 320 (2004).

[20] SNYDER, P.B. et al., Phys. Plasmas **9**, 2037 (2002).

[21] GORMEZANO, C., et al., Nucl. Fusion **47**, S285 (2007).

[22] MURAKMI, M. et al., Phys. Plasmas **13**, 056106 (2006).

[23] HAWRYLUK, R.J., "An Empirical Approach to Tokamak Transport," in *Physics Close to Thermonuclear Conditions*, edited by B. Coppi *et al.* (Commission of the European Communities, Brussels, 1980) Vol. 1, p. 19

[24] HOLCOMB, C.T. et al., "Dependence of Transport on the Safety Factor Profile in DIII-D Steady-State Scenarios," Proc. 37th European Physical Society Conf. on Plasma Physics, Dublin, Ireland, 2010; FERRON, J.R. et al., "Optimization of the Safety Factor Profile for High Noninductive Current Fraction Discharges in DIII-D," these proceedings, EXS/P2-06.

[25] GLASSER, A.H., et al., Am. Phys. Soc. **42**, 1848 (1997).

[26] LAO, L.L., et al., Nucl. Fusion **30** ,1035 (1990).

[27] PANKIN, A., et al., Comput. Phys. Commun. **43** ,61(1981).

[28] LIN-LIU, Y.R., et al., Phys. Plasmas **10**, 4064 (2003).

[29] MAU, T.K., et al., *Radio Frequency Power in Plasmas: 13th Top. Conf.*, American Institute of Physics, Conf. Proc. **485**, New York, 1999, p. 148

[30] MURAKAMI, M. et al., Nucl. Fusion **49**, 065031 (2009).

[31] PARK, J.M., et al., Phys. Plasmas **16**, 092508 (2009).

ACKNOWLEDGMENT

This work was supported in part by the US Department of Energy under DE-AC05-00OR22725, DE-FG02-08ER54984, DE-FC02-04ER54698, DE-FG02-95ER54309 and DE-AC52-07NA27344.